Open access • Journal Article • DOI:10.1002/HLCA.201800120

Understanding Trends in 27Al Chemical Shifts and Quadrupolar Coupling Constants in Chloroalkyl Aluminum [AlClx(Me)3 – x]n = 1 or 2 Compounds

Erwin Lam, Christophe Copéret

Institutions: ETH Zurich

Published on: 01 Sep 2018 - Helvetica Chimica Acta (Wiley)

Topics: Chemical shift

Understanding Trends in Al-27 Chemical Shifts and Quadrupolar Coupling Constants in Chloroalkyl Aluminum [AlClx(Me)(3-x)](n=1 or 2) Compounds

Originally published in:
Helvetica Chimica Acta 101(9), https://doi.org/10.1002/hlca.201800120

Understanding Trends in ^{27}Al Chemical Shifts and Quadrupolar Coupling Constants in Chloroalkyl Aluminum $[AlCl_x(Me)_{3-x}]_{n=1 \text{ or } 2}$ Compounds

Erwin Lam, and Christophe Copéret*

Department of Chemistry and Applied Biosciences, ETH Zürich, Vladimir Prelog Weg 1–5, 8093 Zürich, Switzerland

1 Introduction

Alkyl aluminums are useful reagents in organic synthesis and polymerization catalysis.[1-7] In particular, alkyl aluminum compounds such as diethylaluminum chloride and methylaluminoxane (MAO) and their analogues are ubiquitous co-catalysts in olefin oligomerization and polymerization.[8-13] Several relatively well-defined supported aluminum co-catalysts have been developed in recent years for which one of the major challenges has been their characterization. Amongst advanced spectroscopic methods, solid state ^{27}Al NMR is a very powerful tool to obtain a detailed insight about the structure and the environment of aluminum sites because of the specific chemical shift and quadrupolar coupling constant of ^{27}Al, a spin I = 5/2 nucleus.[14-16] However, the quadrupolar nature of ^{27}Al also yields great challenges due to line broadening that can reach several tens of MHz in the NMR spectrum as the result of interaction between the nuclei with the electric field gradient (EFG). Nowadays, first principles calculations allow reliable evaluation of chemical shift and quadrupolar coupling constants and can thus be used to refine structural assignment in complexes and supported species such as MAO or supported Et_3Al or Et_2AlCl.[17-22] However, those assignments mostly rely on empirical correlation between calculated and experimental data with little understanding on the relation between a given structure and its associated NMR signatures and parameters (chemical shift and quadrupolar coupling constant).[23-26]

Advances in computational chemistry allow now the decomposition of individual components of the chemical shift (and chemical/magnetic shielding) tensor into diamagnetic and paramagnetic contribution; the former is mostly constant for a given nucleus in a broad range of structures and the latter is directly related to the nature and relative energies of the frontier molecular orbitals.[27-29] Such chemical shift analysis helped to obtain a more detailed understanding on how the electronic structure can affect the NMR signature of a given nucleus.

[30-37] The chemical shift (δ) (eq. 1) observed in solution NMR is the average of the principal components from the chemical shift tensor ($\delta_{11} \geq \delta_{22} \geq \delta_{33}$) referenced to the chemical shielding of Al(acac)$_3$ (σ_{iso}^{ref}) and the associated chemical shielding tensor ($\sigma_{11} \leq \sigma_{22} \leq \sigma_{33}$ – eq. 1).

$$\begin{pmatrix} \delta_{11} & 0 & 0 \\ 0 & \delta_{22} & 0 \\ 0 & 0 & \delta_{33} \end{pmatrix} = \sigma_{iso}^{ref} \cdot \begin{pmatrix} 1 & 0 & 0 \\ 0 & 1 & 0 \\ 0 & 0 & 1 \end{pmatrix} - \begin{pmatrix} \sigma_{11} & 0 & 0 \\ 0 & \sigma_{22} & 0 \\ 0 & 0 & \sigma_{33} \end{pmatrix}$$

$$\sigma_{iso} = \frac{1}{3}\,(\sigma_{11} + \sigma_{22} + \sigma_{33}) \qquad (1)$$

Experimentally, Brownian motion averages out the chemical shift anisotropy to its isotropic part in solution and the principal components can only be observed in solid state NMR in the form of a powder pattern. The principal components can be easily extracted from solid state NMR if there are no further effects such as quadrupolar coupling (for I > ½) affecting the line broadening. These principal components can nowadays be also determined by DFT calculations with typically good accuracy along with the chemical shielding tensor (CST) orientation with respect to the molecular structure.[38]

For nuclei with I > ½, the C_Q is associated with an electric field gradient (EFG) tensor (eq. 2), which in its diagonalized form consists of three components following the notation $|V_{33}| \geq |V_{22}| \geq |V_{11}|$.

$$\ddot{\boldsymbol{V}} = \begin{pmatrix} V_{11} & 0 & 0 \\ 0 & V_{22} & 0 \\ 0 & 0 & V_{33} \end{pmatrix} \qquad (2)$$

The tensor is traceless ($V_{11} + V_{22} + V_{33} = 0$) and can be represented by two independent variables: 1) the C_Q which is linearly dependent on V_{33} (eq. 3) with *e* being the electron charge, Q the quadrupole moment of the nuclei and *h* the Planck constant, and 2) the asymmetry parameter η_Q (eq. 4), which describes the symmetry of the electric field gradient around the nucleus.

$$C_Q = (e \cdot Q \cdot |V_{33}|)/h \qquad (3)$$

$$\eta_Q = (V_{11} - V_{22})/\, V_{33} \qquad (4)$$

The C_Q is highly sensitive to the environment and is associated with the charge distribution around the nucleus, which vanishes to zero for isotropic charge distributions.[39-40] Important factors influencing the C_Q are thus the geometry and the ligands linked to the observed nuclei. Herein, we investigate the origin of ^{27}Al NMR parameters for a representative set of molecular chloromethyl aluminum compounds through the analysis of the chemical shielding and quadrupolar coupling constant, relating them to the relative energies and orientation of frontier orbitals, and charge distribution, respectively.

2 Results and Discussion

2.1 ^{27}Al NMR for Aluminum Alkyls and Chlorides.

The NMR parameters of all aluminum monomers and dimers with methyl (-Me) and chloride (-Cl) as substituents are calculated. While the monomers display trigonal aluminum sites (Figure 1a), the most stable dimers have four-coordinated pseudo-tetrahedral aluminum sites with two bridging and two terminal ligands (Figure 1b).

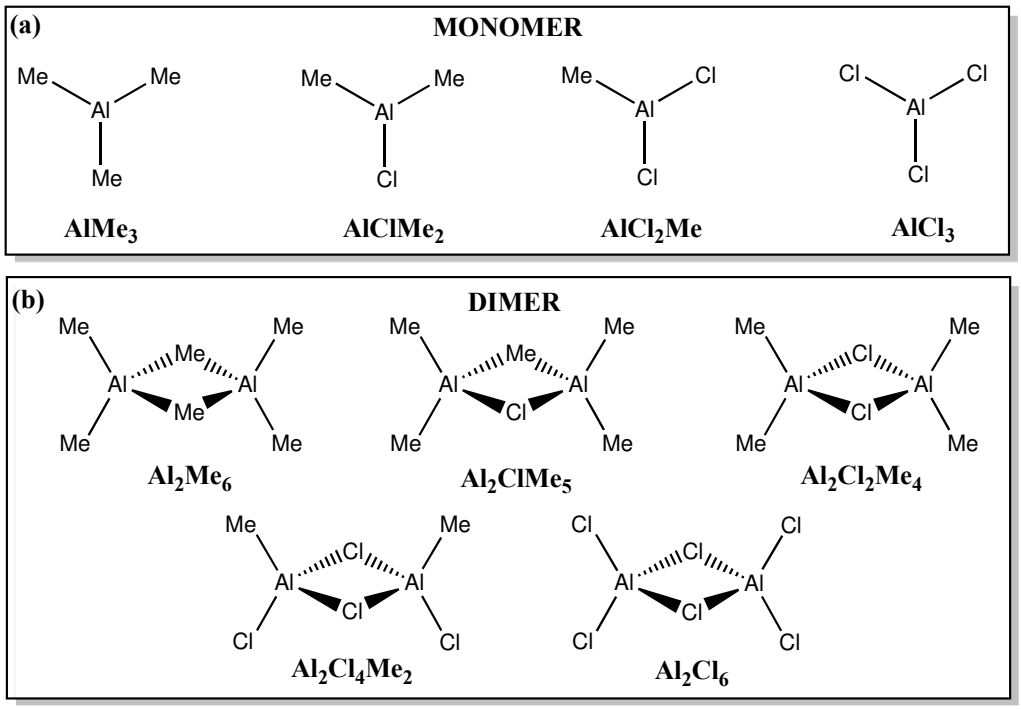

Figure 1. Calculated aluminum monomers (a) and dimers (b) with Me- or Cl-substituents for ^{27}Al NMR calculation.

The calculated NMR parameters are plotted in Figure 2 in the form of isotropic chemical shifts vs C_Q, whose values are consistent with previous reports.[20, 22, 51] For the monomers, the ^{27}Al chemical shift and C_Q values decrease almost linearly as the Me-ligands are substituted by Cl groups (Figure 2 and Table 2), starting at δ_{iso} = 319 ppm and C_Q = 46 MHz for $AlMe_3$ to reach δ_{iso} = 149 ppm and C_Q = 26 MHz for $AlCl_3$. With dimers, the chemical shift and C_Q are in general lower than in the corresponding monomers ($AlMe_3$ vs. Al_2Me_6, $AlClMe_2$ vs. $Al_2Cl_2Me_4$ and $AlCl_3$ vs. Al_2Cl_6). However, when substituting the bridging ligands from μ_2-Me to μ_2-Cl (from Al_2Me_6 to $Al_2Cl_2Me_4$), the chemical shift (δ_{iso}) and in particular the C_Q increase from 160 to 184 ppm and from 24 to 35 MHz, respectively. Changing the terminal ligands to chlorides while having chlorides as bridging ligands (going from $Al_2Cl_4Me_2$ to

Al_2Cl_6) decreases δ_{iso} and the C_Q to 138 ppm and 24 MHz for $Al_2Cl_4Me_2$ and 101 ppm and 14 MHz for Al_2Cl_6. This data set shows that depending on the coordination number and ligand position (bridging vs. terminal), δ_{iso} and C_Q can change in different directions when substituting the Me- with Cl-ligands even with relatively simple model structures of aluminum monomers and dimers.

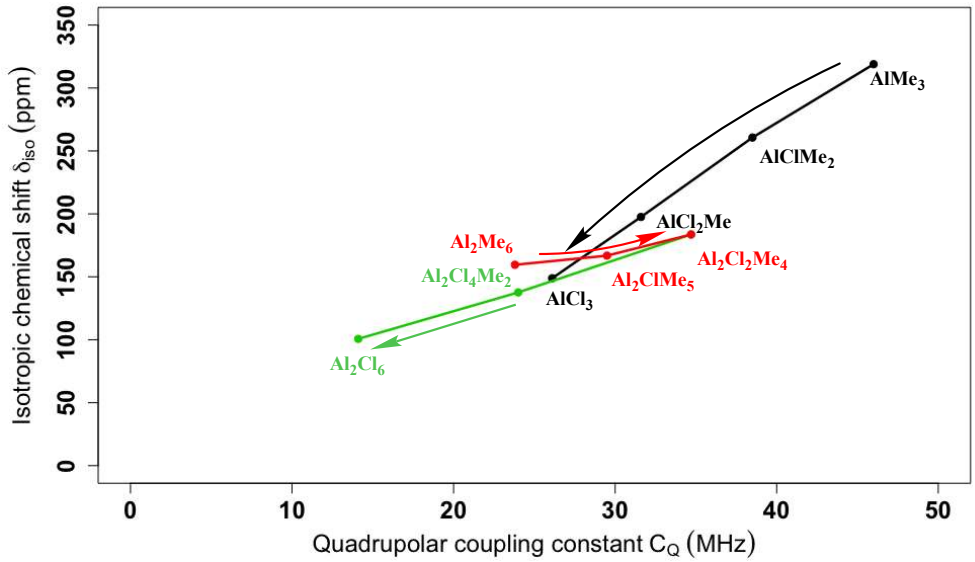

Figure 2. Plot of chemical shift (δ_{iso}) and C_Q for aluminum monomers (black) and aluminum dimers (red and green). The arrows are indicating the change in chemical shift upon substituting the Me- with the Cl-groups of aluminum monomers (black) and the bridging (red) and terminal (green) ligands of aluminum dimers.

In order to understand the observed trends of ^{27}Al NMR parameters (δ_{iso} and C_Q), we carried out a detailed analysis of the origin of the associated principal components. The three principal components of the chemical shift tensors ($\delta_{11} \geq \delta_{22} \geq \delta_{33}$) associated with the chemical shielding tensor ($\sigma_{11} \leq \sigma_{22} \leq \sigma_{33}$) have a specific orientation with respect to the molecular frame. For $AlMe_3$, σ_{33} is along the C_3 axis perpendicular to the plane containing the ligands (referred to as z-axis for all monomeric molecules thereafter – Figure 3). The other two components σ_{22} and σ_{11} lie in the σ_h plane with σ_{22} pointing along one σ-bond and the x-axis while σ_{11} is along the y-axis. The orientation of the chemical shift tensor (σ_{11}, σ_{22} and σ_{33}) changes with respect to the x-, y- and z-molecular axis when substituting methyl by chloride ligands (Figure 3a). This is particularly evident for the component along the z-axis, which is the most shielded σ_{33}

component for $AlMe_3$, the most deshielded one (σ_{11}) for $AlCl_3$, and σ_{22} for $AlClMe_2$ and $AlCl_2Me$ (Figure 3b).

Worthy of note is that the component along the z-axis remains relatively constant for different monomers (Figure 3b). For the aluminum dimers, the z-axis is defined as the axis perpendicular to the plane containing the two aluminum atoms and the two μ_2-briding ligands; the x-axis is co-linear with the axis containing the two aluminum atoms and the y-axis is perpendicular to it (Figure 3c). The principal components of the chemical shielding tensor ($\sigma_{11} \leq \sigma_{22} \leq \sigma_{33}$) also adopt specific orientations with respect to the x-, y- and z-axes. For Al_2Me_6, σ_{11} and σ_{22} lie along the y- and x-axes, respectively. The component σ_{33} points always along the z-axis and is significantly more shielded than σ_{11} and σ_{22} (Figure 3d), which have similar values; hence their orientation with respect to x- and y- axis readily changes depending on the ligands. This orientation is general for all aluminum dimers except for Al_2ClMe_5 where σ_{11} and σ_{22} are oriented almost 45° with respect to the x- and y-axis and along the Al-ligand bond. For all the aluminum dimers, σ_{11} and σ_{22} are following the same trend as σ_{iso}, while σ_{33} is rather constant indicating that σ_{11} and σ_{22} are mainly responsible for influencing the change in chemical shift (Figure 3d).

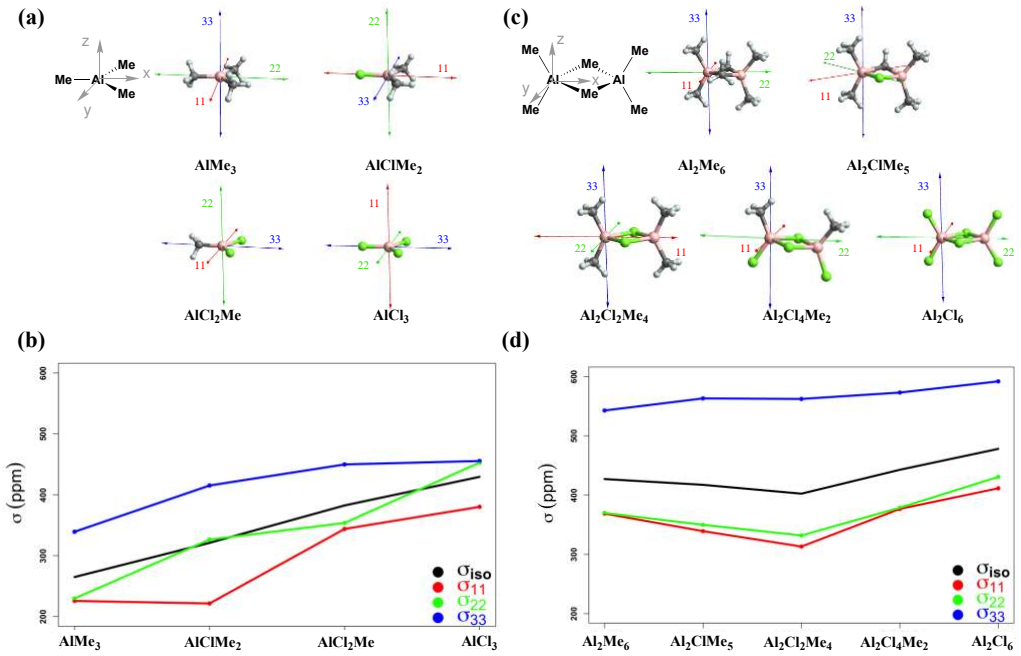

Figure 3. Orientation of the principal components of the chemical shielding tensor for aluminum monomers (a) and the evolution of σ_{iso}, σ_{11}, σ_{22} and σ_{33} (b). Orientation of the principal components of the chemical shielding tensor for aluminum dimers (c) and the evolution of σ_{iso}, σ_{11}, σ_{22} and σ_{33} (d).

In order to understand the origin of the variation in chemical shielding as a function of ligand set, each component is further divided in its diamagnetic contribution (σ_{dia}) and its paramagnetic contribution that includes spin-orbit coupling (σ_{para}).

$$\sigma = \sigma_{dia} + \sigma_{para} \qquad (5)$$

The σ_{para} term, which mostly leads to deshielding, relates to the coupling between virtual and occupied molecular orbitals according to eq. 6. The nominator describes the coupling of occupied (occ) and virtual (virt) orbitals via action of the angular momentum operator $\hat{L}_i$ (i = x, y, and z). The denominator ($\Delta E_{virt-occ}$) describes the energy difference between the coupled orbitals, thus indicating that the orbitals closest in energy – the frontier molecular orbitals – mostly contribute to the paramagnetic term, hence relating electronic structure to chemical shielding and chemical shift.

$$\sigma_{para} \sim \sum_{occ}\sum_{virt} \frac{\langle\psi_{virt}|\hat{L}_i|\psi_{occ}\rangle\langle\psi_{virt}|\hat{L}_i/r^3|\psi_{occ}\rangle}{\Delta E_{virt-occ}} \qquad (6)$$

In the case of main group elements like aluminum, paramagnetic shielding/deshielding will arise from the coupling of *p*-orbitals; its magnitude can be readily evaluated by a simple examination of the molecular orbital diagram and in a pictorial way by examining the overlap

between *p*-orbitals in occupied and virtual orbitals upon a rotation of 90° around the axis associated with the specific angular momentum operators, $\hat{L}_x$, $\hat{L}_y$ and $\hat{L}_z$ (vide infra).

2.2 Natural Chemical Shielding Analysis for ^{27}Al Monomers.

Since the principal components of the chemical shielding tensor ($\sigma_{11} \leq \sigma_{22} \leq \sigma_{33}$) change their orientation with respect to the molecular axis for different aluminum monomers (Figure 3a), it is easier to compare them by their relative orientation to the molecular axis and use the corresponding σ_{xx}, σ_{yy} and σ_{zz} component. This approach also facilitates a comparison between them because of their similar structure and associated frontier molecular orbitals (vide infra). For all calculated aluminum monomers, the changes in chemical shielding can be solely interpreted in terms of variation of σ_{para}, because σ_{dia} is similar in all cases

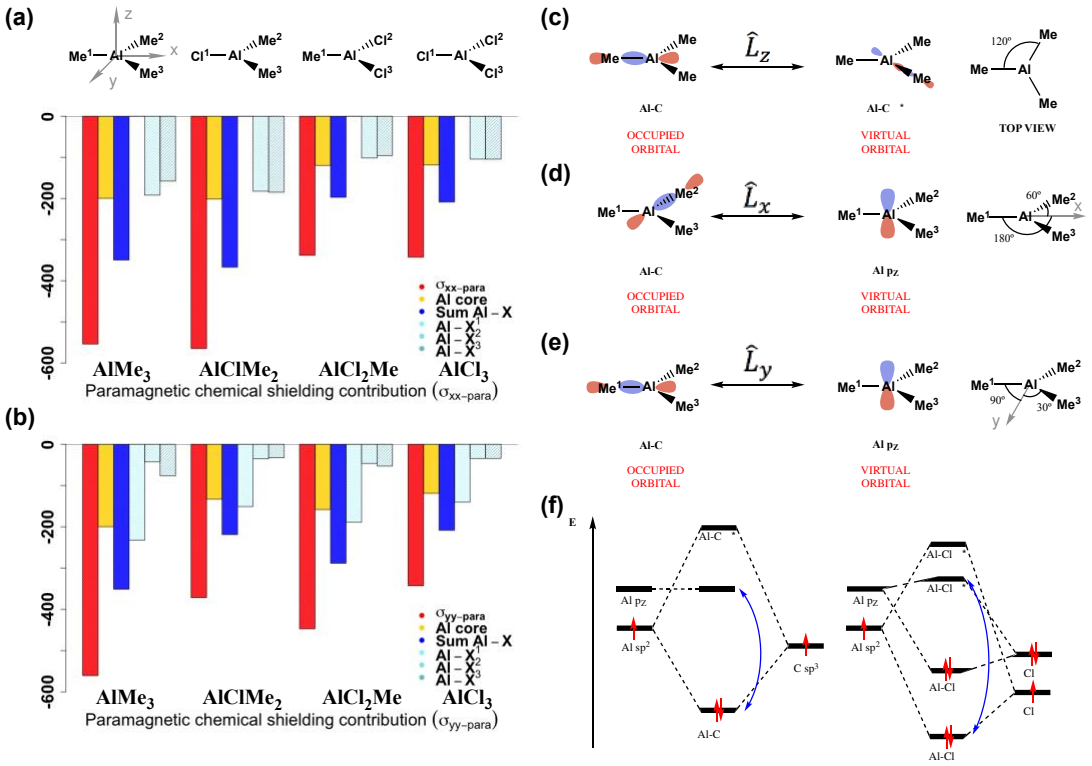

Figure 4. Contribution from natural localized molecular orbitals (NLMO) to the paramagnetic part of the chemical shielding for (a) σ_{xx} and (b) σ_{yy} of the aluminum monomers with the total paramagnetic chemical shielding (red), the contribution of the Al-core (yellow), the summed Al-X σ-orbital (X=Me or Cl) (blue) and their individual contribution (lightblue). Effect of the angular momentum operator on Al-C σ-orbitals of (c) $\hat{L}_z$, (d) $\hat{L}_x$ and (e) $\hat{L}_y$. (f) Orbital diagram of Al-C and Al-Cl σ-bond with the blue arrow indicating the main interaction leading to deshielding in ^{27}Al NMR.

(Figure 7- 10 and Table 3). The evolution of the paramagnetic contribution (σ_{para}) of the principal components ($\sigma_{xx\text{-}para}$, $\sigma_{yy\text{-}para}$ and $\sigma_{zz\text{-}para}$) shows that $\sigma_{zz\text{-}para}$ (Figure 11 and Table 4) is relatively constant and that the changes are dominated by these of $\sigma_{xx\text{-}para}$ (Figure 4a) and $\sigma_{yy\text{-}para}$ (Figure 4b) on going from $AlMe_3$ to $AlCl_3$. Note that the evolution of $\sigma_{xx\text{-}para}$ and $\sigma_{yy\text{-}para}$ are complementary (Figure 12) due to the symmetry of the molecules and are best discussed concomitantly. In order to understand how $\sigma_{ii\text{-}para}$ (i = x, y and z) change along the series ($AlMe_3$ to $AlCl_3$), a natural chemical shielding (NCS) analysis is carried out to identify which orbitals contribute to shielding/deshielding (Figure 4a- 4b). From $AlMe_3$ to $AlClMe_2$, with Cl along the x-axis the term $\sigma_{xx\text{-}para}$ (Figure 4a) remains the same, but $\sigma_{yy\text{-}para}$ (Figure 4b) becomes significantly less deshielded due to a lower contribution of the Al–X_1 σ-orbital as the Al-Me_1 bond is replaced by an Al-Cl_1 bond (Figure 4b).

Upon replacing one more Me- by a Cl-ligand in $AlCl_2Me$, $\sigma_{xx\text{-}para}$ is now reduced greatly due to reduced Al σ-orbital contributions (Figure 3a and 4a), while the term $\sigma_{yy\text{-}para}$ lies in between these found in $AlMe_3$ and $AlClMe_2$ (Figure 4b). Finally, replacing the last Me-ligand on going from $AlCl_2Me$ to $AlCl_3$, $\sigma_{yy\text{-}para}$ is now further reduced. Overall, the replacement of each Me by Cl decreases $\sigma_{xx\text{-}para}$ and $\sigma_{yy\text{-}para}$.

The origin of this trend can be understood by analyzing which occupied and virtual orbitals couple upon action of the angular momentum operator $\hat{L}_i$ ($\hat{L}_x$, $\hat{L}_y$ and $\hat{L}_z$ related to $\sigma_{xx\text{-}para}$, $\sigma_{yy\text{-}para}$ and $\sigma_{zz\text{-}para}$). This can be illustrated by using $AlMe_3$ as an example. The operator $\hat{L}_z$ allows coupling between Al-C σ-orbitals and neighboring Al-C σ*-orbitals (Figure 4c), but since the Me-Al-Me angles are 120° while an optimal overlap is achieved when the orbitals are perpendicular to each other, coupling between them will only be partial. The operators $\hat{L}_x$ and $\hat{L}_y$ allow coupling between the Al-C σ-orbital and the empty *p*-orbital on aluminum. Due to the C_3 axis, the Al-C bonds are not always oriented perpendicular to $\hat{L}_x$ (Figure 4d) or $\hat{L}_y$ (Figure 4e) making the coupling between the Al-C σ-orbital and the empty *p*-orbital not optimal.

Similar coupling partners for each individual component are found for all aluminum monomers (Figure 3), but their contribution is modulated by the change from the Me- to the more electronegative Cl-ligands. Substituting Me- with the more electronegative Cl-ligands lowers the energy of the Al–X σ-orbital and also slightly increases the energy of the *p*-orbital due to interactions of the empty Al *p*-orbital with Cl-lone pairs (Al-Cl π∗-orbital) as illustrated in a qualitative orbital diagram in Figure 4f. As a consequence, σ_{xx} and σ_{yy} undergo a lower deshielding with increasing number of Cl-ligands consistent with the observed upfield chemical shift on going from $AlMe_3$ to $AlCl_3$.

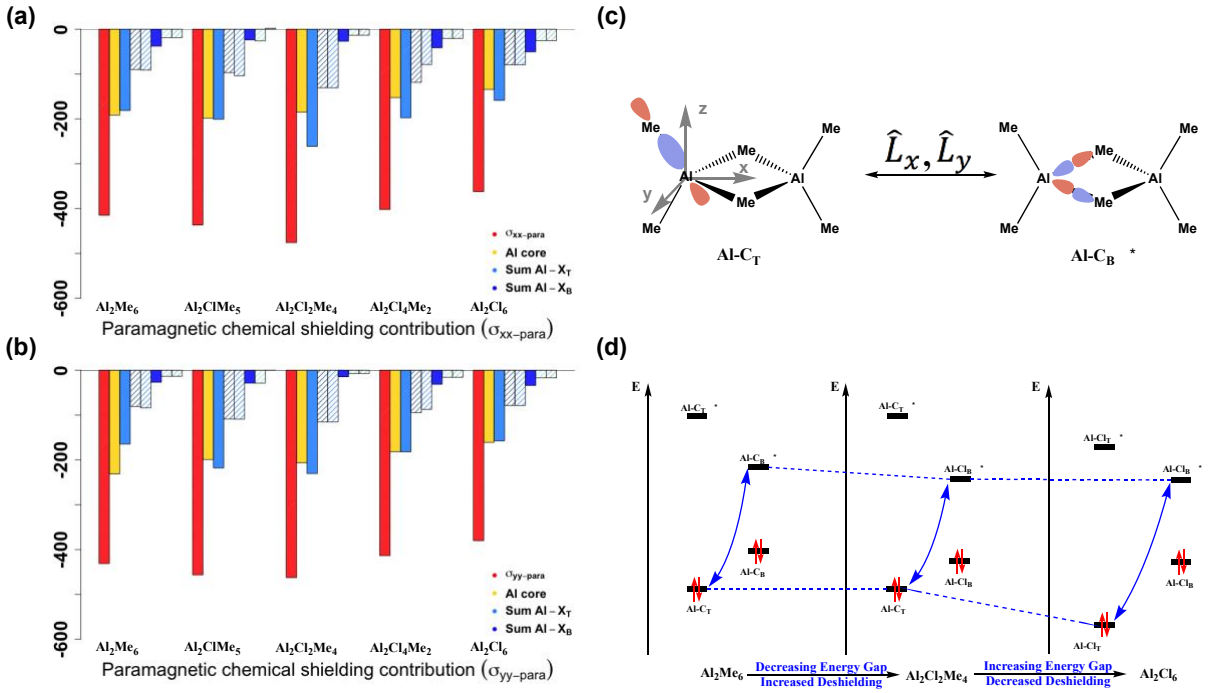

Figure 5. Contribution from natural localized molecular orbitals (NLMO) to the paramagnetic part of the chemical shielding for (a) σ_{xx} and (b) σ_{yy} of the aluminum dimers with the total paramagnetic chemical shielding (red), the contribution of the Al-core (yellow), the summed terminal Al-X_T σ-orbital (X_T=Me or Cl) (lightblue) and bridging Al-X_B σ-orbital (X_B=Me or Cl) (blue) with their individual contribution. (c) Effect of the angular momentum operator on Al-Cl σ-orbitals of $\hat{L}_x$ and $\hat{L}_y$ illustrated by Al_2Me_6. (d) Orbital diagram of orbitals which are mainly contributing to the change in chemical shift of aluminum dimers (Al-X σ and Al-X σ* (X=C or Cl)) indicated by a blue arrow of Al_2Me_6 to $Al_2Cl_2Me_4$ and $Al_2Cl_2Me_4$ to Al_2Cl_6.

2.3 Natural Chemical Shielding Analysis for ^{27}Al Dimers.

Similar to what is observed for the aluminum monomers, the change of chemical shielding is mostly due to the paramagnetic term for aluminum dimers. These changes in chemical shielding are mainly related to $\sigma_{xx\text{-para}}$ (Figure 5a) and $\sigma_{yy\text{-para}}$ (Figure 5b), while $\sigma_{zz\text{-para}}$ is relatively constant across the series (Figure 13- 15 and Table 5). NCS analysis reveals that the change of σ_{para} is mostly related to the terminal X_T group, as the contributions from the bridging Al-X_B σ-orbitals are generally small (Figure 5a- 5b and Table 6). The terminal Al-X_T σ-bonding orbitals are coupled through the angular momentum operators $\hat{L}_x$ and $\hat{L}_y$ to the Al-X_B σ*-orbital of the bridging ligands (Figure 5c). Therefore, substituting the bridging ligands of Al_2Me_6 with chlorides ($Al_2Cl_2Me_4$) increases the Al-X_T σ-orbital contribution due to the lower lying σ*-orbitals in the bridging Al-Cl bond (Figure 5d). Substituting the terminal

Me- with Cl-ligands (on going from $Al_2Cl_2Me_4$ to $Al_2Cl_4Me_2$ and from $Al_2Cl_4Me_2$ to Al_2Cl_6) provides lower lying Al–X_T σ-orbitals and thereby decreases the Al-X_T σ-orbital contribution leading to less deshielding (Figure 5d).

2.4 Quadrupolar Coupling in ^{27}Al NMR.

For all aluminum monomers, $AlMe_3$ displays the largest V_{33} (1.4) that is directed along the empty *p*-orbital of aluminum, and C_Q (46 MHz) with η_Q equal to 0.0 consistent with its axial symmetry. The large C_Q highlights the large charge imbalance that originates from the presence of anionic ligands in the σ_h plane leading to a negative tensor component shown in orange in Figure 6a and to the presence of empty *p*-orbital along the z-axis leading to a positive tensor component (blue region in Figure 6a). Replacing one Me- with a Cl-ligand decreases V_{33} (1.2) and the C_Q (39 MHz), and increasing the number of Cl-ligands in $AlCl_2Me$ or $AlCl_3$ further decreases V_{33} and C_Q to 1.0 and 32 MHz for $AlCl_2Me$, and to 0.8 and 26 MHz for $AlCl_3$, respectively (Figure 6a and Table 7). The decrease of C_Q value with increasing number of more electron accepting Cl-ligands is consistent with the expected reduced electron density around Al in the x,y-plane containing these ligands. In addition, the Cl-ligand can also donate electron density to the empty *p*-orbital perpendicular to the plane by interaction with its lone pair (π-interaction), which further leads to a more isotropic charge distribution around aluminum. This is shown by a reduced positive contribution from the Al-Cl bond and a negative contribution from the Cl-lone pair after decomposing V_{33} in individual NLMO contributions and consistent with what is reported for $AlMe_3$ and $AlCl_3$[40, 51] (Figure 6a).

All aluminum dimers have significantly lower C_Q than the monomers, in line with the pseudo-tetrahedral geometry of Al and the associated more uniform distribution of charges. The orientation of V_{33} is along the z-axis for all dimers except $Al_2Cl_4Me_2$ that is slightly off the z-axis. In contrast to the aluminum monomers, V_{33} corresponds to a negative EFG tensor component.

From Al_2Me_6 to Al_2-(μ_2-Cl)$_2Me_4$, V_{33} is decreasing from -0.7 to -1.1, which corresponds to a C_Q of 24 MHz and 35 MHz (Figure 6b and Table 8). Changing the terminal ligands ($Al_2Cl_2Me_4$ to Al_2Cl_6), V_{33} is going from -1.1 to -0.4 and the associated C_Q decreases from 35 MHz to 14 MHz. The trends in V_{33} are associated to how the charge imbalance is evolving with respect to the ligands. For Al_2Me_6 the coplanar region around the bridging ligands and aluminum is associated to a positive charge imbalance. Therefore substituting the bridging Me-ligands with more electron accepting Cl-ligands will lead to an increased positive charge (larger charge imbalance) around aluminum and an increase in C_Q. On the other hand, the region along

the terminal ligands is associated to a negative charge imbalance and having more electron accepting Cl-ligands at this position leads to a decrease in C_Q. In addition, the Al-X (X = Me or Cl) bond lengths only have a minor influence on the C_Q (Table 9), showing that altering all the bond lengths at the same time does not generate a large charge imbalance compared to changing the ligands. Overall the EFG tensor (with the associated C_Q) can thus sensitively probe the charge imbalance i.e. regions with increased positive and negative charge.

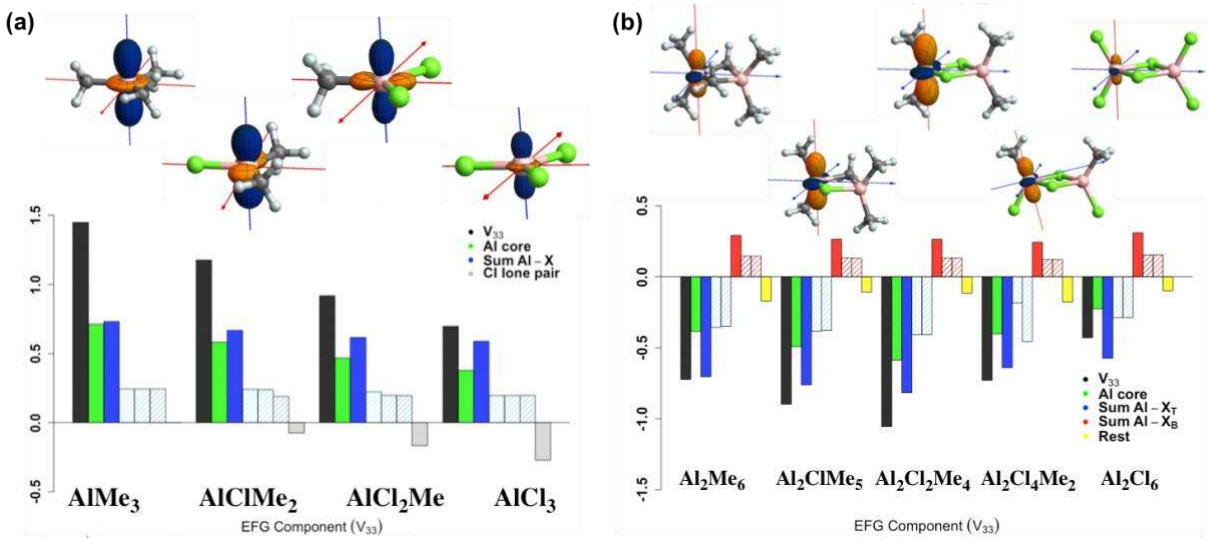

Figure 6. Polar plot and orientation of the EFG tensor of aluminum monomers (a) and dimers (b) and the individual contribution to V_{33} (black) from natural localized molecular orbitals (NLMOs) corresponding to the Al-core (green), the summed Al-X bond (X=Me or Cl) (blue) their individual contribution (light blue), contributions from the Cl-lone pair (grey) and the remaining contributions (yellow). For the dimers, the ligand contributions are further divided into summed terminal Al-X_T bond (X_T=Me or Cl) (blue) with their individual contribution (light blue) and the summed bridging Al-X_B bond (X_B=Me or Cl) (red) with their individual contribution (light red).

3 Conclusion

DFT calculation of ^{27}Al NMR of aluminum monomers and dimers bearing Me- or Cl-ligands show peculiar trends between the chemical shift and C_Q with the ligand set and geometry, which can be understood at the molecular level upon analysis of their principal components. The chemical shift and C_Q decrease for trigonal planar aluminum with substitution of Me- with Cl-ligands, whereas for the dimers, depending on whether the terminal or bridging ligands are substituted from Me- to Cl-ligands, the inversed trend is observed (increase in

chemical shift and C_Q when substituting Me- with Cl-ligands for bridging ligands and decrease for terminal ligands). First, a natural chemical shielding analysis shows that all the observed trends in chemical shift can be explained by the small changes in energy of σ-bonding Al–X orbitals, the empty *p*-orbital for the monomers or the σ*-orbitals for the dimers: i) the increasing number of Cl ligands in the monomer decreases the energy of the σ-orbitals and raises this of the empty *p*-orbital, hence the decrease of chemical shift in this series and ii) the presence of Cl as bridging ligand lowers the energy of the σ*, hence the increase of chemical shift upon going from Al_2Me_6 to Al_2-(μ_2-Cl)$_2Me_4$, before decreasing with increasing number of Cl-terminal ligands due to the lowering of the Al-X σ-orbital energies. In case of the C_Q for ^{27}Al, where a similar trend as for the chemical shift is observed, it can be rationalized by the charge distribution, where a more uniformly distributed charge distribution leads to a lower C_Q. In particular, for trigonal planar aluminum less σ-donating ligands (Me vs. Cl) and ligands with lone pair donating electron density into the empty *p*-orbital (Cl) lead to a reduced C_Q, while for four coordinated aluminum dimers a lower C_Q is observed when placing more σ-donating ligands (Me-ligands) at the bridging position and less σ-donating ligands (Cl-ligands) at the terminal position. This chemical shift and charge distribution analysis implies that chloroalkyl aluminum compounds would be more reactive among the dimers as it shows very polarizable bonds. This may explain why such reagents are preferred as activators in homogeneous catalysis.[52]

4 Epilogue

Chloroalkyl aluminums display specific reactivity patterns depending on the number of Cl-ligands. First, the Lewis acidity of $AlCl_xMe_{3-x}$ increases with the number of Cl atoms (Table 10). This contrasts with what is observed for chemical shift principal components lying along the σ_h plane and the quadrupolar coupling constant, which all decrease with increasing number of Cl atoms in part because of the associated vacant *p*-orbital. This illustrates that Lewis acidity is not correlated with the energy of the vacant *p*-orbital as one may have anticipated. This is also in sharp contrast to what is observed for both the ^{15}N and ^{27}Al NMR for the pyridine adducts, whose upfield NMR chemical shift (Figure 16) directly parallels the increase of Lewis acidity.[53] Worthy of note, Al_2-(μ_2-Cl)$_2Me_4$ is often a better co-catalysts by comparison with Al_2Me_6 for oligomerization catalysts.[52] This pattern correlates well with the highest C_Q value among all dimeric species. In fact, the high C_Q value describes the polarization of this dimeric

species, which is probably critical as the proposed role of these dimeric alkyl aluminium species is to transfer an alkyl group, but also to capture and stabilize the associated aluminum species.

5 Computational Details

Geometry optimization and frequency calculations were performed with the B3LYP[41] functional in combination with the 6-31g(d)[42] basis set using the Gaussian09[43] program suite. Chemical shift calculations were performed with the ADF 2014[44] code using a TZP[45] basis set with the all-electron relativistic zeroth-order regular approximation (ZORA)[46-47] in its spin-orbit two-component form. EFGs were calculated using a TZP basis set.[40] For all the calculations with ADF 2014 the revised Perdew-Burke-Entzerhof (revPBE)[48-49] functional was used. For the natural localized molecular orbitals (NLMO) analysis of the chemical shielding principal components and V_{33}, the NBO 6.0[50] code is used as implemented in ADF 2014 with the revPBE functional and TZP basis set. The chemical shift of ^{27}Al is referenced to $Al(acac)_3$ (0.0 ppm). Using two experimentally measured compounds[51], namely $Al(Mes)_3$ and $Al(NTMS)_3$ as benchmark calculations shows that the methodology in use is able to accurately calculate the trends in C_Q of three coordinated aluminum centers (Table 1).

6 References

[1] D. Y. Kondakov, E.-i. Negishi, *J. Am. Chem. Soc.* **1996**, *118*, 1577-1578.

[2] D. Y. Kondakov, E.-i. Negishi, *J. Am. Chem. Soc.* **1995**, *117*, 10771-10772.

[3] E. Negishi, D. E. Van Horn, T. Yoshida, *J. Am. Chem. Soc.* **1985**, *107*, 6639-6647.

[4] G. A. Olah, *Angew. Chem., Int. Ed.* **2003**, *32*, 767-788.

[5] E. i. Negishi, *Chem. Eur. J.* **1999**, *5*, 411-420.

[6] E.-i. Negishi, *Dalton Trans.* **2005**, 827-848.

[7] S. D. Aldrige, A.J., in *The Group 13 Metals Aluminium, Gallium, Indium and Thallium: Chemical Patterns and Peculiarities*, John Wiley & Sons, Ltd., Chichester, U.K., **2011**.

[8] W. Kaminsky, *Macromolecules* **2012**, *45*, 3289-3297.

[9] H. S. Zijlstra, S. Harder, *Eur. J. Inorg. Chem.* **2015**, *2015*, 19-43.

[10] M. Brasse, J. Cámpora, M. Davies, E. Teuma, P. Palma, E. Álvarez, E. Sanz, L. Reyes Manuel *Advanced Synthesis & Catalysis* **2007**, *349*, 2111-2120.

[11] A. Boudier, P.-A. R. Breuil, L. Magna, H. Olivier-Bourbigou, P. Braunstein, *Dalton Trans.* **2015**, *44*, 12995-12998.

[12] Z. Boudene, A. Boudier, P.-A. R. Breuil, H. Olivier-Bourbigou, P. Raybaud, H. Toulhoat, T. de Bruin, *J. Catal.* **2014**, *317*, 153-157.

[13] S. D. C. Fliedel, Springer Berlin Heidelberg, Berlin, Heidelberg, **2013**, pp. 125-171.

[14] A. Kermagoret, R. N. Kerber, M. P. Conley, E. Callens, P. Florian, D. Massiot, F. Delbecq, X. Rozanska, C. Copéret, P. Sautet, *J. Catal.* **2014**, *313*, 46-54.

[15] R. Wischert, P. Florian, C. Copéret, D. Massiot, P. Sautet, *J. Phys. Chem. C* **2014**, *118*, 15292-15299.

[16] D. R. Neuville, L. Cormier, D. Massiot, *Chem. Geol.* **2006**, *229*, 173-185.

[17] E. Zurek, C. J. Pickard, J. Autschbach, *J. Phys. Chem. C* **2008**, *112*, 11744-11750.

[18] J. Joubert, F. Delbecq, P. Sautet, E. L. Roux, M. Taoufik, C. Thieuleux, F. Blanc, C. Copéret, J. Thivolle-Cazat, J. M. Basset, *J. Am. Chem. Soc.* **2006**, *128*, 9157-9169.

[19] A. Kermagoret, R. N. Kerber, M. P. Conley, E. Callens, P. Florian, D. Massiot, C. Coperet, F. Delbecq, X. Rozanska, P. Sautet, *Dalton Trans.* **2013**, *42*, 12681-12687.

[20] R. N. Kerber, T. Kerber, X. Rozanska, F. Delbecq, P. Sautet, *Phys. Chem. Chem. Phys.* **2015**, *17*, 26937-26945.

[21] Z. Falls, E. Zurek, J. Autschbach, *Phys. Chem. Chem. Phys.* **2016**, *18*, 24106-24118.

[22] R. N. Kerber, A. Kermagoret, E. Callens, P. Florian, D. Massiot, A. Lesage, C. Copéret, F. Delbecq, X. Rozanska, P. Sautet, *J. Am. Chem. Soc.* **2012**, *134*, 6767-6775.

[23] C. Bonhomme, C. Gervais, F. Babonneau, C. Coelho, F. Pourpoint, T. Azaïs, S. E. Ashbrook, J. M. Griffin, J. R. Yates, F. Mauri, C. J. Pickard, *Chem. Rev.* **2012**, *112*, 5733-5779.

[24] S. E. Ashbrook, D. M. Dawson, *Acc. Chem. Res.* **2013**, *46*, 1964-1974.

[25] A. Pedone, *Int. J. Quantum Chem.* **2016**, *116*, 1520-1531.

[26] R. E. Wasylishen, in *Calculation of NMR and EPR Parameters*, Wiley-VCH Verlag GmbH & Co. KGaA, **2004**, pp. 433-447.

[27] C. M. Widdifield, R. W. Schurko, *Concepts Magn. Reson. Part A* **2009**, *34A*, 91-123.

[28] N. F. Ramsey, *Phys. Rev.* **1950**, *78*, 699-703.

[29] J. B. Grutzner, in *Recent Advances in Organic NMR Spectroscopy* (Ed.: J. B. R. Lambert, R.), Norell Press, Landisville, **1987**, pp. 17-42.

[30] C. P. Gordon, K. Yamamoto, W.-C. Liao, F. Allouche, R. A. Andersen, C. Copéret, C. Raynaud, O. Eisenstein, *ACS Cent. Sci.* **2017**, *3*, 759-768.

[31] S. Halbert, C. Copéret, C. Raynaud, O. Eisenstein, *J. Am. Chem. Soc.* **2016**, *138*, 2261-2272.

[32] D. P. Estes, C. P. Gordon, A. Fedorov, W.-C. Liao, H. Ehrhorn, C. Bittner, M. L. Zier, D. Bockfeld, K. W. Chan, O. Eisenstein, C. Raynaud, M. Tamm, C. Copéret, *J. Am. Chem. Soc.* **2017**, *139*, 17597-17607.

[33] K. Yamamoto, P. Gordon Christopher, W. C. Liao, C. Copéret, C. Raynaud, O. Eisenstein, *Angew. Chem., Int. Ed.* **2017**, *56*, 10127-10131.

[34] C. P. Gordon, K. Yamamoto, K. Searles, S. Shirase, R. A. Andersen, O. Eisenstein, C. Coperet, *Chem. Sci.* **2018**, *9*, 1912-1918.

[35] E. Lam, A. Comas-Vives, C. Copéret, *J. Phys. Chem. C* **2017**, *121*, 19946-19957.

[36] J. Autschbach, S. Zheng, *Magn. Reson. Chem.* **2008**, *46*, S45-S55.

[37] S. Berger, W. Bock, G. Frenking, V. Jonas, F. Mueller, *J. Am. Chem. Soc.* **1995**, *117*, 3820-3829.

[38] R. W. Schurko, R. E. Wasylishen, A. D. Phillips, *J. Magn. Reson.* **1998**, *133*, 388-394.

[39] A. J. Rossini, R. W. Mills, G. A. Briscoe, E. L. Norton, S. J. Geier, I. Hung, S. Zheng, J. Autschbach, R. W. Schurko, *J. Am. Chem. Soc.* **2009**, *131*, 3317-3330.

[40] J. Autschbach, S. Zheng, R. W. Schurko, *Concepts Magn. Reson. Part A* **2010**, *36A*, 84-126.

[41] A. D. Becke, *J. Chem. Phys.* **1993**, *98*, 5648-5652.

[42] W. J. Hehre, R. Ditchfield, J. A. Pople, *J. Chem. Phys.* **1972**, *56*, 2257-2261.

[43] M. J. T. Frisch, G. W.; Schlegel, H. B.; Scuseria, G. E.; Robb, M. A.; Cheeseman, J. R.; Scalmani, G.; Barone, V.; Mennucci, B.; Petersson, G. A.; Nakatsuji, H.; Caricato, M.; Li, X.; Hratchian, H. P.; Izmaylov, A. F.; Bloino, J.; Zheng, G.; Sonnenberg, J. L.; Hada, M.; Ehara, M.; Toyota, K.; Fukuda, R.; Hasegawa, J.; Ishida, M.; Nakajima, T.; Honda, Y.; Kitao, O.; Nakai, H.; Vreven, T.; Montgomery, J. A., Jr.; Peralta, J. E.; Ogliaro, F.; Bearpark, M.; Heyd, J. J.; Brothers, E.; Kudin, K. N.; Staroverov, V. N.; Kobayashi, R.; Normand, J.; Raghavachari, K.; Rendell, A.; Burant, J. C.; Iyengar, S. S.; Tomasi, J.; Cossi, M.; Rega, N.; Millam, J. M.; Klene, M.; Knox, J. E.; Cross, J. B.; Bakken, V.; Adamo, C.; Jaramillo, J.; Gomperts, R.; Stratmann, R. E.; Yazyev, O.; Austin, A. J.; Cammi, R.; Pomelli, C.; Ochterski, J. W.; Martin, R. L.; Morokuma,K.;Zakrzewski,V.G.;Voth,G.A.;Salvador,P.; Dannenberg, J. J.; Dapprich, S.; Daniels, A. D.; Farkas, Ö.; Foresman, J. B.; Ortiz, J. V.; Cioslowski, J.; Fox, D. J., Wallingford, CT, **2009**.

[44] G. te Velde, F. M. Bickelhaupt, E. J. Baerends, C. Fonseca Guerra, S. J. A. van Gisbergen, J. G. Snijders, T. Ziegler, *J. Comput. Chem.* **2001**, *22*, 931-967.

[45] P. L. Barbieri, P. A. Fantin, F. E. Jorge, *Mol. Phys.* **2006**, *104*, 2945-2954.

[46] C. Chang, M. Pelissier, P. Durand, *Phys. Scr.* **1986**, *34*, 394-404.

[47] E. v. Lenthe, E. J. Baerends, J. G. Snijders, *J. Chem. Phys.* **1993**, *99*, 4597-4610.

[48] J. P. Perdew, K. Burke, M. Ernzerhof, *Phys. Rev. Lett.* **1996**, *77*, 3865-3868.

[49] Y. Zhang, W. Yang, *Phys. Rev. Lett.* **1998**, *80*, 890-890.

[50] E. D. B. Glendening, J. K.; Reed, A. E.; Carpenter, J., J. A. M. E.; Bohmann, C. M.; Landis, C. R.; Weinhold, F.*, Vol. 2013*, Theoretical Chemistry Institute, University of Wisconsin: Madison, WI,, **2013**.

[51] J. A. Tang, J. D. Masuda, T. J. Boyle, R. W. Schurko, *ChemPhysChem* **2006**, *7*, 117-130.

[52] A. Kermagoret, P. Braunstein, *Organometallics* **2008**, *27*, 88-99.

[53] I. B. Moroz, K. Larmier, W.-C. Liao, C. Copéret, *J. Phys. Chem. C* **2018**, *122*, 10871-10882.